Available online at www.sciencedirect.com

ScienceDirect

Physics Procedia 83 (2016) 249 – 257

Physics Procedia

9th International Conference on Photonic Technologies - LANE 2016

Picosecond laser surface cleaning of AM1 superalloy

D. Moskal[a,*], J. Martan[a], M. Kučera[a], Š. Houdková[a], R. Kromer[b]

[a]*New Technologies - Research Centre, University of West Bohemia in Pilsen, 306 14 Plzeň, Czech Republic*
[b] *Université Bourgogne Franche-Comté, UTBM, IRTES EA7274, 90010 Belfort, France*

Abstract

Laser scanning processing of nickel-based superalloy AM1 surfaces by ultra-short pulses (10 ps) is introduced as a cleaning and deoxidation postprocess. The laser cleaning is investigated with two-directional surface scanning by a laser beam with several frequencies of pulse generation. The EDX elemental analyses of the laser cleaned AM1 surfaces were compared with the non-laser treated surface. The optimal speed, laser pulse repetition frequency, overlapping and layer repetition count are determined for minimal structural changes on the mechanically polished AM1 surfaces. The laser cleaning after shifted laser surface texturing (sLST) is presented as a two-step preparation of a superalloy surface for thermal spraying. The heat accumulation effect and temperature fields are calculated from a semi-planar model of a laser beam scanning heat source. The theoretical results are discussed in comparison with experimental studies. The upper and bottom bounds are defined for an optimal high speed laser cleaning process.

Peer-review under responsibility of the Bayerisches Laserzentrum GmbH

Keywords: superalloy surface cleaning; ultra-short laser pulses; scanning process optimization; postprocessing; shifted texturing

1. Introduction

Laser pulse scanning processing technology is widely used for the cleaning of oxidized or contaminated surfaces (Kumar et al., 2013; Lee and Watkins, 2000; Mandolfino et al., 2015; Garbacz et al. 2010). Ultra-short pulse laser processing of the materials provides cleaning of metal surfaces without cracks, critical structural changes or deep oxidation of metals (Bauer et al., 2015; Jaeggi et al., 2014; Neuenschwander et al., 2014). The main parameters of

* Corresponding author. Tel.: +420-726-914-724 .
E-mail address: moskal@ntc.zcu.cz

Peer-review under responsibility of the Bayerisches Laserzentrum GmbH
doi:10.1016/j.phpro.2016.08.020

the scanning strategy are laser spot overlapping, pulse energy, frequency and scanning speed (Neuenschwander et al., 2014; Neuenschwander et al., 2015). The optimal scanning strategy parameters play a key role in the case of the laser processing of materials with specific structural properties, such as superalloys (Reed, 2015; Zuhlke et al., 2013; Liu et al., 2013; Zhang et al., 2013).

In this article, results of the ultra-short pulse cleaning of the superalloy AM1 surface with different laser beam scanning parameters are presented. The optimal parameters of the laser scanning technology are applied as post processing cleaning of the superalloy AM1 after shifted laser surface texturing (sLST) (Moskal et al., 2015). The temperature field distribution and temperature increase due to heat accumulation are calculated from the heat conduction equation with a semi-planar model of laser beam heat source, which is similar to the thermal model presented by Weber et al. (2014).

Nomenclature

T	temperature;
t	time;
z	distance from surface in the depth of material;
F_{Heat}	heat source fluence;
ΔT	temperature changes;
ρ	material density;
c	specific heat;
α	thermal diffusivity;
F_0	laser fluence in the center of the laser spot;
P	total power in the laser beam;
r	distance from the laser spot center to the point on the scanned surface;
ω_0	beam half-width;
η	fraction coefficient of absorption;
n	number of laser pulses applied over fixed point;
N	full number of the laser pulses over fixed point;
r_n	distance between fixed point and center of the applied laser spot;
t_n	time, when the laser pulse with index n is applied.

2. Experimental setup

2.1. Equipment and material

A picosecond laser with pulse length 10 ps, quality of the laser beam $M^2 \leqslant 1.3$ and wavelength 532 nm was used (X25-2-G from EdgeWave GmbH). The maximal pulse energies were set from 31.05 μJ at frequency 500 kHz to 2.09 μJ at frequency 4 MHz (see Table 1). The optical scheme contains laser beam expander 2-8x, and scanhead intelliSCAN® III 14 with 255 mm focal length f-theta objective (SCANLAB AG). The maximal laser beam scanning speed in this configuration is equal to 8 m/s. In the applied scanning technique, several repeated bidirectional line scanning layers were used for material processing. For the scanhead position used, repeatability is <0.5 μm and this has no significant influence on the cleaning process result.

The profiles of the structural changes on the laser scanned surfaces were done with 3D digital microscope HIROX KH-7700. The more precision structural investigations, surface oxidation value and laser induced ripples were done with SEM FEI Quanta 200 and an EDX analyzer. The superalloy samples were disc-shaped, with a diameter of 19.6 mm and a thickness of about 1.7 mm. The surface was mechanically polished with a 9 um diamond suspension. The EDX elemental composition of the mechanically polished surface was: O = 0.41 %, Al = 6.86 %, Si = 4.75 %, Ti = 1.1 %, Cr = 6.87 %, Co = 6.39 %, Ni = 59.8 %, Ta = 6.25 %, W = 2.57 %, Mo = 4.99 %. The EDX elemental composition was controlled for three stages of the superalloy surface: the initial surface, laser cleaned

surface and laser overheated surface. The laser cleaned surface means the laser scanned surface with removal of the thin surface layer without significant oxidation or structural changes of the residual surface. In contrast for it, the laser overheated surface means the laser scanned surface with increased oxygen concentration and significant structural changes, such as remelting or other phase changes.

Table 1. Laser pulse parameters for different frequencies of the laser generation.

Frequency (kHz)	4000	2000	1333	1000	800	667	571	500
Pulse energy (μJ)	2.09	5.79	9.90	14.1	18.32	22.60	26.85	31.05
Pulse fluence (J/cm2)	0.30	0.82	1.40	1.99	2.59	3.20	3.80	4.40

2.2. The laser scanning technique

The spot diameter in all the experiments presented was 30 μm and the laser spot inline overlapping was changed by changing of the frequency. The diameter of the laser spot was determined experimentally by optical microscopy from a non-overlapped one line-laser path at maximal pulse energy and maximal scan speed. The scanning hatch contains two perpendicular hatches with a distance between the lines equal to 13 μm. These hatch parameters correspond to 47% of overlapping between hatch lines. This overlapping value gives maximal scanning speed with minimal visible scanning lines. In the case when overlapping is bigger, the scanning lines are not visible, but processing time of the one scan layer increases. With an increase of the hatch lines' distance, the processing time of one scan decreases, but the scanning lines become more noticeable and the surface does not have metallic shining. The laser pulse energy increases for lower frequency of laser generation and this was taken into account for the analyses of the integral fluence value (Table 2.). Whole experiments have 40 scanning layers with the maximal speed of the laser beam equal to 8 m/s. This technique is similar to studies of nickel-based superalloy processing by femtosecond laser (Semaltianos et al. 2008, see item 3.1).

Table 2. Overlapping and laser integral fluence for scanning speed 8 m/s.

Parameters set number	I	II	III	IV	V	VI	VII	VIII
Frequency (kHz)	500	571	667	800	1000	1333	2000	4000
Inline spots distance (μm)	16	14	12	10	8	6	4	2
Inline spots overlapping (%)	46.67	53.30	59.96	66.67	73.33	80.00	86.87	93.33
Integral fluence for one layer (J/cm^2)	14.94	14.75	14.48	14.09	13.56	12.69	11.13	8.04
Heat accumulation temperature increase (K)	434	431	424	422	412	400	380	300

The software of the Galvano scanner offers two control strategies to synchronize the scan pattern with gating of the laser source – delays optimization and the "SkyWriting" method. The first one was used for the uninterrupted transition from the highest speed laser processing to the lowest speed processing by tuning the parameter "LaserOff" delay at the edges of the scanning field. When the parameter "LaserOff" is too long, then the laser is not switched off after the scan head mirrors start to decelerate. This technique with a higher value of the "LaserOff" parameter was used for the comparative analysis of the experimental difference between the laser processed and initial surfaces. For this experiment the frequency was the same 500 kHz which corresponds to the maximal used pulse fluence of 31.05 J/cm^2 (parameters set number is I in Table 2).

The second technique of the laser processing (named "SkyWriting") has no deceleration effect and the scanning speed is constant for the whole scanning field. The "SkyWriting" technique was in use for the experiments with a frequency spectrum from 4 MHz down to 500 kHz of the laser pulse generation (Table 2). The last row in Table 2 was obtained by theoretical calculations, which are described in section 3.2.

One scanned field has a rectangular form with height 5 mm and width 30 mm. The minimal time between application of two neighbor hatched lines is equal to 40 ms. Full time processing of one scan layer is equal to 3 sec.

3. Results and discussion

3.1. Initial mechanically polished and laser beam scanned surfaces

The experiment with the delays optimization technique has shown that the picosecond laser beam scanning is preferential to provide the highest speed for superalloy surface polishing. It is demonstrated by scanning of the superalloy surface with increased delay parameter "LaserOff". The mechanically polished initial surface is presented at the top area in Fig. 1 (areas 1 - 2). The oxygen content is presented in the white-numbered squares in Fig. 1, where it was typically detected. The content of oxygen for the mechanically polished surface is about 0.41 %. It is bigger in comparison with the laser scanned surface (Fig. 1, areas 6 - 7), but smaller in comparison with the edge area of the scanned field (Fig. 1, areas 3 - 5).

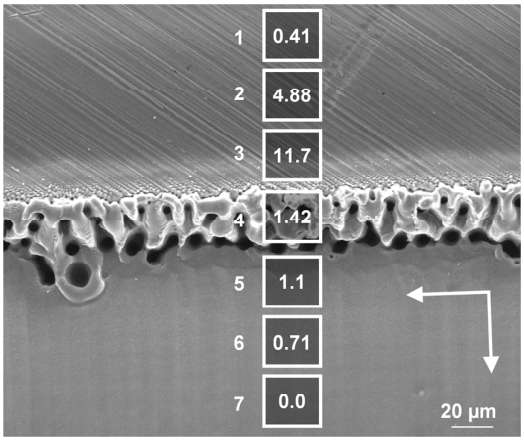

Fig. 1. SEM image of superalloy surface with boarder area between mechanically polished and laser scanned surfaces. In the white-numbered squares, the content of oxygen is indicated in (%). White arrows show scanning beam directions and the parameters set number is I in Table 2.

The frequency of the laser pulse generation is 500 kHz in this case and it is about 47 % of the laser spot overlapping (see Table 2, parameters set number I). These parameters of the scanning are very close to the fine method of nickel-based superalloy laser cleaning, because the tracks of mechanical polishing disappeared and oxygen content vanished here (Fig. 1, area 7). However, this regime does not work correctly on the mechanically polished superalloy surface which contains initial defects, such as cracks and pores, before laser scanning (Fig. 2, *a*). During the process of surface scanning, peaks start to grow on the edges of these initial defects (Fig. 2, *b*). The mechanism of the peaks' growth can be explained by the initial surface defects affecting the laser beam energy distribution and they function as precursor sites for the above-surface-growth (ASG) structures (Zuhlke et al. 2013). Formation of these structures strongly depends on the repetition rate, laser pulse fluence and speed of scanning (Semaltianos et al. 2008 and Zuhlke et al. 2013).

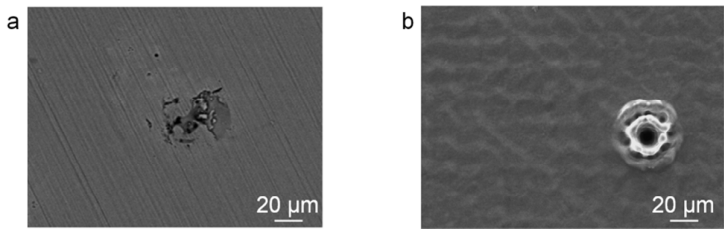

Fig. 2. (a) SEM image of superalloy surface with an initial surface defect after mechanical polishing; (b) SEM image of superalloy laser polished surface which contains a pore with above-surface-growth (ASG) structures around it (parameters set number is I in Table 2).

Similar structures appeared on the edge area of the scanning field, where movement of the mirrors is decelerated and overlapping of the laser pulses increased until laser beam scanning is stopped (Fig. 1, area 4). The slow speed of the scanning leads to a high heat accumulation temperature increase and, as a result, laser-induced porous structures appear. Formation of these structures under picosecond laser pulses on stainless steel and under femtosecond laser pulses on a superalloy is discussed by Liu et al. (2013) and Zuhlke et al. (2013). The mechanism of the formation of these structures was described as overheated liquid explosion under laser pulses with fluence F>1.2 J/cm^2 and 1 kHz repetition rate (Liu et al., 2013, pp. 7-8).

At higher frequencies the energy of the laser pulse is smaller, but higher overlapping and shorter time between pulses decrease the ablation threshold of the metal surface, as was investigated by Raciukaitis et al. (2008). The next part of this study was aimed at the regression of the peaks growth with higher frequencies of laser pulse generation. In Fig. 3, surfaces for several frequencies of the laser generation which are presented in the Table 2 are shown. The concentration of oxygen was not higher than 0.2 % for all laser scanned surfaces.

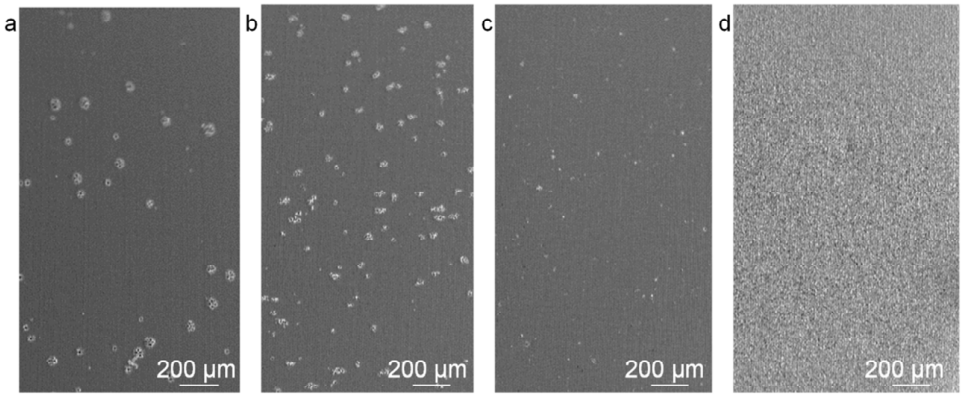

Fig. 3. SEM images taken from superalloy surfaces scanned by laser beams with different pulse frequencies: (a) 500 kHz, parameters set number is I in Table 2; (b) 1 MHz, parameters set number is V in Table 2; (c) 2 MHz, parameters set number is VII in Table 2; (d) 4 MHz, parameters set number is VIII in Table 2.

The maximal suppression of the peak formation was achieved at the frequency equal to 2 MHz (parameters set number is VII in Table 2). There are no ASG structures on the pores and their edges become more smoothed (Fig. 4). The laser pulse fluence for this regime is 0.82 J/cm^2 and it agrees with limitation fluent value <1.2 J/cm^2 for thermal peak growth, mentioned by Liu et al. (2013), pp. 7-8.

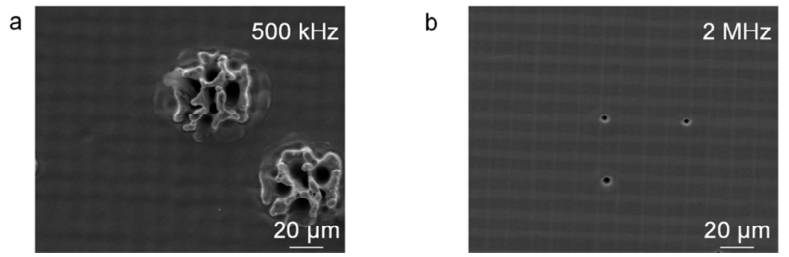

Fig. 4. (a) SEM image taken from superalloy surface with laser induced structural peaks around initial surface defects at 500 kHz, parameters set number is I in Table 2; (b) SEM image taken from superalloy surface with laser polished surface and smoothed initial pores at 2 MHz, parameters set number is VII in Table 2.

The laser beam scanning of a superalloy surface with 2.0 MHz frequency is an optimal regime, because scanning with a higher frequency initiated surface degradation (Fig. 3, d; parameters set number is VII in Table 2). Estimated throughput for the cleaning process is about 2.5 cm^2/min (40 layers of scanning). At frequency 4 MHz, formation of ASG structures is not suppressed. This fact leads to the conclusion that there is a lower boundary for ASG structure suppression. In this study this lower boundary was found to be equal to 0.30 J/cm^2.

3.2. Semi-planar model of scanning a Gaussian heat source

There is a well-known theory for temperature distribution from an instantaneous plane source presented by Carslaw and Jaeger (1959). The task of determining the temperature distribution $T(t,z)$ in a semi-infinite medium at the depth z from an instantaneous plane heat source with strength F_{Heat}, parallel to the plane x and applied at the time $t=0$ is formulated (Carslaw and Jaeger, 1959; Balageas et al., 1986):

$$\Delta T(t,z)=\frac{F_{Heat}e^{-z^2/4\cdot\alpha\cdot t}}{\rho\cdot c\cdot\sqrt{\pi\cdot\alpha\cdot t}} \tag{1}$$

where $\Delta T(t,z)$ - temperature changes, ρ - material density, c - specific heat capacity, t - time, and α - thermal diffusivity. Here the value F_{Heat} is only part of the laser pulse energy. For ultra-short laser pulses, the main part of the laser pulse energy is taken away by reflection, vaporization and ablation processes. The residual part of the thermal energy F_{Heat} can be defined as part of the laser pulse energy F value by fraction coefficient $\eta=F_{Heat}/F$. It is almost impossible to provide a theoretically accurate determination of the fraction coefficient η. The reason is the number of physical processes activated at the moment of laser pulse absorption: the dynamic of laser pulse interaction with material, (super)heating, vaporization and material ablation with thermal and phase-transformation changes of the material properties. The fraction coefficient was measured in experiments with a calorimetric setup (Bauer et al., 2015) and by fitting of experimental results (Weber et al., 2014). In this work, the fraction coefficient was assumed to be equal to 12.5%, as for a nickel-based alloy, mentioned by Weber et al. (2014).

Laser fluence in the laser spot is described by the Gaussian function (Hecht, 2002, pp. 594-596):

$$F=F_0\cdot e^{-2\cdot r/\omega_0} \tag{2}$$

where F - laser fluence (J/cm^2), F_0 - laser fluence in the center of the laser spot, which is equal to $F_0=2\cdot P/(\pi\cdot\omega_0^2)$, P - total power in the beam, r - distance from the laser spot center, and ω_0 - beam half-width. The short time of the laser pulse and the small gradient of the laser fluence in the micrometer scale (about 0.01 J/cm^2) give the possibility to divide the temperature distribution task into several semi-planar tasks. This means that it is possible to describe temperature distribution from every point in the laser spot as temperature distribution from several independent planar heat sources, with laser fluence calculated from equation (2). This assumption simplifies the temperature distribution problem. In this case the resulting equation for the temperature history for any surface point inside of the laser spot has the form:

$$\Delta T(t,z)=\frac{\eta\cdot F_0 e^{-\frac{2r}{\omega_0}-\frac{z^2}{4\cdot\alpha\cdot t}}}{\rho\cdot c\cdot\sqrt{\pi\cdot\alpha\cdot t}} \tag{3}$$

For a scanned laser beam it is convenient to take a fixed point on the material surface and track the temperature changes during laser beam movement across it. Every laser pulse in the scanned beam involves heat energy depending on the distance from this fixed point to the center of the laser spot, according to equation (1). Summary temperature at this fixed point from all laser pulses is calculated from equation:

$$\Delta T_{Sum}(t,z)=\left(\eta\cdot F_0\Big/\rho\cdot c\cdot\sqrt{\pi\cdot\alpha}\right)\cdot\sum_{n=1}^{N} e^{-\frac{2r}{\omega_0}-\frac{z^2}{4\cdot\alpha\cdot(t-t_n)}}\Big/\sqrt{t-t_n} \tag{4}$$

where n - number of laser pulses applied over a fixed point, N - full number of the laser pulses over the fixed point, which were applied till actual time t, r_n - distance between the fixed point and center of the applied laser spot, and t_n - time when the laser pulse with index n is applied.

Heat accumulation temperature increase is an important parameter of laser processing. The value of the heat accumulation temperature increase is evaluated as the temperature increase of the surface at a fixed point at the last moment before application of the next laser pulse in the sequence. Equation 4 was used for determination of temperature changes and heat accumulation for all frequencies which were in use in the experimental tests. The resulting temperature histories for a point fixed at coordinate $x=0$ on a scanning line with frequencies 4 MHz (parameters set number is VIII in Table 2) and 2 MHz (parameters set number is VII in Table 2) of the laser pulses are presented in Fig. 5. The starting temperature for calculations was assumed to be 25° C. The time step in the calculations was 10 ps, like the laser pulse length. The highest temperature of laser scanning processing reached up to unphysically high values, when laser shots were applied closely to the fixed point on the surface, but for evaluation of heat accumulation it is enough to take into account only temperatures under the melting point. This presented model describes the distribution of residual heat only for the solid part of the laser processed material. The heat energy which was spent for (super)heating, vaporization, ablation, etc. is considered in fraction coefficient η.

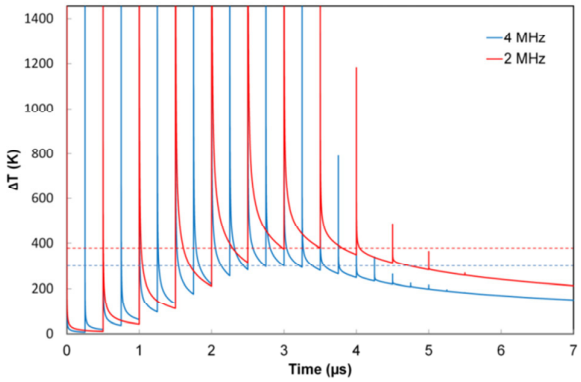

Fig. 5. Numerical calculations of surface temperature changes and heat accumulation temperature increase at a fixed point on the surface of the superalloy for 4 MHz (parameters set number is VIII in Table 2, dotted blue line corresponds to maximal heat accumulation 300 K) and for 2 MHz (parameters set number is VII in Table 2, dotted blue line corresponds to maximal heat accumulation 380 K).

Most interesting is frequency 2 MHz for fine laser polishing of the superalloy. Here the maximal heat accumulation temperature increase is reached at 380 K (Fig. 5, red line). Lower heat accumulation up to 300 K was determined for higher frequency of the laser generation (Fig. 5, blue line), but this regime did not lead to a clear laser polishing of the surface (see Fig. 3, *d*). This can be explained by the decrease of the damage threshold at a higher repetition rate, as mentioned by Jaeggi et al. (2011) and lower effectiveness of thermal energy distribution on the surface, as shown by Neuenschwander et al. (2014) and Sailer et al. (2015). The heat accumulation value for all

used frequencies of laser pulse generation is presented in Table 2 in the last row. Laser cleaning of the superalloy surface is very sensitive to the temperature regime of processing. The increase or decrease of the heat accumulation temperature in the region 20÷80 K has a dramatic influence on the structural changes of the superalloy surface. This can be seen from the comparison of structural changes (Fig. 3) with calculation results (Table 2).

3.3. Application of laser surface cleaning for a textured superalloy surface

A special technique of laser surface texturing called shifted laser surface texturing (sLST) is in use for preparation of stainless steel and superalloy surfaces for thermal spray processing (Kromer et al., 2016; Moskal et al., 2015). The laser processing of a superalloy involves heat effects on the surface and precipitation of evaporated material near the laser spot, as observed by Feng et al. (2004) and Petronic et al. (2011). Though sLST does not involve a heat accumulation effect, precipitation on the surface occurs (Fig. 6, *a*). Cleaning of the superalloy surface after sLST was provided as postprocessing with optimal parameters of laser beam scanning. This postprocessed surface of the superalloy has no precipitation or plasma condensing layer (Fig. 6, *b*).

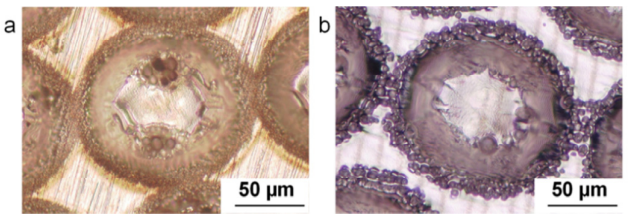

Fig. 6. Multifocal optical images of superalloy sLST dimples without laser cleaning (a) and with laser cleaning postprocessing (cleaning parameters set number is VII in Table 2) (b).

4. Conclusion

This paper has presented an analysis of the influence of process parameters on laser surface cleaning of superalloy AM1. Optimal parameters of the scanning process were found. Optimal overlapping of the laser spots is about 86.7% at the laser fluence equal to 0.82 J/cm2. The calculated heat accumulation temperature increase for these optimal parameters is up to 380 K. It was found that small changes of the heat accumulation temperature increase in the region of 20÷80 K strongly affects the resulting morphology of the superalloy surface. Laser cleaning outside the optimal scanning regime involves formation of ASG structures. The upper boundary of optimal laser fluence lies near 1.2 J/cm^2 and the lower boundary for suppression of ASG structures was estimated as equal to 0.30 J/cm^2. Optimal parameters of laser beam cleaning were successfully applied for a superalloy AM1 surface after sLST as postprocessing. Laser surface cleaning as preprocessing and higher laser fluence with a low repetition rate for providing quality sLST will be areas for further research.

Acknowledgements

The result was developed within the CENTEM project, reg. no. CZ.1.05/2.1.00/03.0088, co-funded by the ERDF as part of the Ministry of Education, Youth and Sports of the Czech Republic OP RDI programme and, in the follow-up sustainability stage, supported through CENTEM PLUS (LO1402) by financial means from the Ministry of Education, Youth and Sports under the ”National Sustainability Programme I” and project SGS-2016-005.

References

Balageas, D.L., Krapez, J.C., Cielo, P., (1986). Pulsed photothermal modeling of layered materials. J. Appl. Phys. 59, 348-357. doi:10.1063/1.336690.

Bauer, F., Michalowski, A., Kiedrowski, T., Nolte, S., (2015). Heat accumulation in ultra-short pulsed scanning laser ablation of metals. Opt. Express 23, 1035–1043. doi:10.1364/OE.23.001035.

Carslaw, H.S., Jaeger, J., (1959). Conduction of heat in solids, second edi. ed. Oxford at the Clarendon Press.

Feng, Q., Picard, Y.N., Liu, H., Yalisove, S.M., Mourou, G., Pollock, T.M., (2004). Femtosecond laser micromachining of a single-crystal superalloy. Mater. Sci. 53, 511–516. doi:10.1016/j.scriptamat.2005.05.006.

Garbacz, H., Koss, A., Marczak, J., Mróz, J., Onyszczuk, T., Rycyk, A., Sarzyński, A., Skrzeczanowski, W., Strzelec, M., Zatorska, A., (2010). Optimized laser cleaning of metal artworks–evaluation of determinants. Phys. Procedia 5, 457–466. doi:10.1016/j.phpro.2010.08.168.

Hecht, E., (2002). Optics, 4th ed. Addison-Wesley, San Francisco.

Jaeggi, B., Neuenschwander, B., Schmid, M., Muralt, M., Zuercher, J., Hunziker, U., (2011). Influence of the pulse duration in the ps-regime on the ablation efficiency of metals. Phys. Procedia 12, 164–171. doi:10.1016/j.phpro.2011.03.118.

Jaeggi, B., Neuenschwander, B., Zimmermann, M., Loor, R. De, Penning, L., (2014). High throughput ps-laser micro machining with a synchronized polygon line scanner, in: 8th International Conference on Photonic Technologies LANE 2014. pp. 1–8.

Kromer, R., Costil, S., Cormier, J., Berthe, L., Peyre, P., Courapied, D., (2016). Laser Patterning Pretreatment before Thermal Spraying: A Technique to Adapt and Control the Surface Topography to Thermomechanical Loading and Materials. J. Therm. Spray Technol. 25, 401–410. doi:10.1007/s11666-015-0352-x.

Kumar, M., Bhargava, P., Biswas, A.K., Sahu, S., Mandloi, V., Ittoop, M.O., Khattak, B.Q., Tiwari, M.K., Kukreja, L.M., (2013). Epoxy-paint stripping using TEA CO 2 laser: Determination of threshold fluence and the process parameters. Opt. Laser Technol. 46, 29–36. doi:10.1016/j.optlastec.2012.04.021.

Lee, J.M., Watkins, K.G., (2000). In-process monitoring techniques for laser cleaning. Opt. Lasers Eng. 34, 429–442. doi:10.1016/S0143-8166(00)00073-7.

Liu, B., Wang, W., Jiang, G., Mei, X., Wang, K., Wang, J., (2013). Formation of porous structure with subspot size under the irradiation of picosecond laser pulses. J. Nanomater. 2013. doi:10.1155/2013/301301.

Mandolfino, C., Lertora, E., Genna, S., Leone, C., Gambaro, C., (2015). Effect of laser and plasma surface cleaning on mechanical properties of adhesive bonded joints. Procedia CIRP 33, 458–463. doi:10.1016/j.procir.2015.06.054.

Moskal, D., Kučera, M., Smazalová, E., Houdková, Š., Kromer, R., (2015). APPLICATION OF SHIFTED LASER SURFACE TEXTURING 1–6.

Neuenschwander, B., Jaeggi, B., Schmid, M., Hennig, G., (2014). Surface structuring with ultra-short laser pulses: Basics, limitations and needs for high throughput. Phys. Procedia 56, 1047–1058. doi:10.1016/j.phpro.2014.08.017.

Neuenschwander, B., Jaeggi, B., Zimmermann, M., Markovic, V., Resan, B., Weingarten, K., de Loor, R., Penning, L., (2015). Laser Surface Structuring with 100W of Average Power and Sub-ps Pulses, in: International Congress on Applications of Lasers & Electro-Optics (ICALEO). pp. 14–22.

Petronic, S., Milosavljevic, A., Sedmak, A., Djeric, A., Nikolic, J., (2011). Analysis of damages of superalloys arrisen by lasers that operate in different pulse regimes, in: The 9th International Conference Structural Integrity of Welded Structures. pp. 1–7.

Raciukaitis, G., Brikas, M., Gecys, P., Gedvilas, M., (2008). Accumulation effects in laser ablation of metals with high-repetition- rate lasers Gediminas. Spie 7005, 70052L–70052L–11. doi:10.1117/12.782937.

Reed, R.C., (2015). The Superalloys: Fundamentals and Applications, The effects of brief mindfulness intervention on acute pain experience: An examination of individual difference. doi:10.1017/CBO9781107415324.004.

Sailer, M., Bauer, F., Kleiner, J., Kaiser, M., (2015). Scaling of Ablation Rates . Ablation Efficiency and Quality Aspects of Burst-Mode Micromachining of Metals.

Semaltianos, N.G., Perrie, W., French, P., Sharp, M., Dearden, G., Watkins, K.G., (2008). Femtosecond laser surface texturing of a nickel-based superalloy. Appl. Surf. Sci. 255, 2796–2802. doi:10.1016/j.apsusc.2008.08.043.

Weber, R., Graf, T., Berger, P., Onuseit, V., Wiedenmann, M., Freitag, C., Feuer, A., Negel, J., Voss, A., Abdou Ahmed, M., Bauer, D., Sutter, D., Killi, A., Graf, T., (2014). Heat accumulation during pulsed laser materials processing. Opt. Express 22, 11312–11324. doi:10.1364/OE.22.011312.

Zhang, W., Cui, X., Feng, Q., Cheng, G., Ma, G., Zhang, X., (2013). Pyramid-like spikes in a single crystal superalloy produced by picosecond laser irradiation. Appl. Phys. A Mater. Sci. Process. 113, 373–377. doi:10.1007/s00339-013-7968-9.

Zuhlke, C. a, Anderson, T.P., Alexander, D.R., (2013). Formation of multiscale surface structures on nickel via above surface growth and below surface growth mechanisms using femtosecond laser pulses. Opt. Express 21, 8460–8473. doi:10.1364/OE.21.008460.